Preliminary Study on Wireless Passive Resistive Sensor Applied for Smart Objects

Michela Borghetti, Edoardo Cantù, Emilio Sardini, Mauro Serpelloni
Department of Information Engineering
University of Brescia
Brescia, Italy
m.borghetti001@unibs.it, e.cantu@unibs, emilio.sardini@unibs.it, mauro.serpelloni@unibs.it

***Abstract*—Smart objects are capable of measuring the surrounding environment or internal status through their sensors. A viable solution to implement sensors in objects is to print them directly on the object. Printed electronics enables customization in the design and in the choice of the materials according to the final application. Aerosol jet printing (AJP) is a technology for the fabrication of electronic components directly onto objects. In combination with AJP, passive telemetric systems can represent a valid solution to interrogate sensors, reducing the number of electronic components integrated into the object. An example of a scenario on Industry 4.0 is smart packaging, which supports the control of the production process and of the transportation chain. In this work, we propose a manufacturing process based on AJP for fabricating simultaneously the sensing coil and the tuning capacitor to be used in a passive telemetric system for the measurement of a resistive sensor at a fixed frequency. The printed devices were characterized by electrical and geometrical points of view. The printed capacitance can be tuned from 13.95 pF to 31 pF, by changing the number of depositions. Capacitors with the same characteristics differ 1.28% at maximum. For validation, printed coil and printed capacitor were then used in a telemetric system for measuring resistive loads; known commercial resistors were used and the maximum error between the nominal value and the measured value obtained by the telemetric system was lower than 6% in the range 2.2 kΩ and 560 kΩ.**

Keywords—Telemetric system; printed coil; printed antenna; printed capacitor; resistive sensor; smart object; aerosol jet printing.

I. Introduction

Internet of Things (IoT) is one of the most appealing topics in many sectors. For example, it can be adopted to provide information about industrial production processes and to improve safety [1], to monitor the health and to support the early detection of medical issues [2], or to collect data for smart homes and smart cities [3]. IoT is a network of different smart devices that can collect and analyze data, and share information with other devices [4]. Among IoT devices, smart objects represent an interesting category of objects, because they are everyday objects with a specific function, but they are equipped with "intelligence" (sensors, computational ability, storage, *etc.*) [5]. Smart objects can be adopted in industrial contests to improve efficiency, maintenance, and traceability. For example, in [6] a smart cutting tool equipped with Fiber Bragg grating sensors was employed to detect cutting forces in harsh machining environments and to monitor tool condition and machining process. The assessment of service quality can be performed by the measurement of the condition of the environment/items (temperature, humidity, gas content, etc.), and the transformation of traditional packages into smart devices is obtained through the integration of multiple sensors and electronics. For example, a traceability system based on smart tags is proposed to track food conditions during transportation by monitoring the temperature [7].

The object becomes "smart" when sensors or electronic devices are implemented on the object, but sometimes the installation of commercial devices is challenging due to geometrical constraints or materials compatibility. Furthermore, in some applications, specific requirements need the design of custom solutions, and they can include the fabrication of the electronic components directly onto the object [9]. In this regard, printed electronics (PE) can offers innovative technologies to design and fabricated sensors and electronics according to the specific context and application. However, the possibility of printing electronics and sensors directly onto 3D is still challenging and requires innovative printing technologies. Among the printed technologies, Aerosol jet printing (AJP) is capable of integrating electronics and sensors directly onto objects also on 3D shapes, without installation or assembly. This is a viable solution in several applications, such as in autonomous smart devices.

In Industry 4.0, an autonomous device that communicates wirelessly is preferred, when cables and wires could not reach the measurement device or the installation and the replacement of batteries are challenging. For example, in smart packaging applications, only sensors capable of measuring temperature, humidity, and the presence of volatile amine compounds, to estimate food freshness should be installed on the package and should be interrogated wirelessly [8]. Passive telemetric systems based on a passive sensor (resistive or capacitive) and a coil coupled with a readout coil could represent a valid solution to read in real-time passive sensors [9]. For example, in [10] a paper-based single printed spiral coil sensor was proposed to monitor humidity levels in a pillbox, and in [11] a passive wireless spiral coil sensor was proposed to measure the surface temperature sensor. In both cases, a sweep in frequency is required to read the output of the sensor. In [9], a telemetric method based on the impedance reading at a specific frequency is proposed to a resistive temperature sensor, but this method required a tuning capacitor to adjust the impedance. Furthermore, in [11], [12] the fabrication method is not suitable to fabricate the device directly onto the objects with a non-planar surface, such as rectangular hinged food containers or a jar. AJP is capable of printing components and sensors directly onto objects. In an AJP system, the atomizer (viscosity ranging 1-1000 cP) creates a dense mist of material (the droplets are of 1-5 microns diameter) starting from the liquid ink (of viscosity ranging from 1 cP to 1000 cP). The aerosol mist is focused by a sheath gas, which surrounds the aerosol as an annular ring inside the deposition head, from the nozzle to the substrate over a distance of 2 to 5 mm. The resolution of the printed lines ranges from 10 µm to millimeters [5]. Furthermore, AJP is capable to deposit both conductive and insulating materials for the fabrication of capacitors.

In this work, AJP is proposed to fabricate a coil and a tuning capacitor for the development of a passive telemetric system for Industry 4.0 and smart packaging applications. Since AJP is a relatively new technology, a further investigation on the properties of the ink, on the design (Section II), and on the manufacturing process (Section III) is required to manufacturing passive electronic components. In Section IV, the printed coil and the capacitor were tested from the electrical and geometrical points of view, and they were used in a passive telemetric system to measure resistive components.

II. Design of the Sensing Coil

A. Theoretical Background

According to [9], the resistive sensor to be measured is connected to a tuning capacitor and a sensing coil, which is magnetically coupled with an external readout coil (Fig. 1a). In this application, all the components of the sensing part are printed directly onto a lid, and the resistance R_x of the resistive sensor could be calculated through the measurement of the impedance Z at the readout terminals. The sensor could be a resistive humidity sensor, a temperature sensor, or a piezoresistive sensor (for the pressure of force measurement). As discussed previously in [9], the electronic components could be modeled with lumped elements (L_1, C_1, R_1 for the readout inductor, L_2, R_2, C_2 for the sensing inductor, C_x for the tuning capacitor, R_x for the resistive sensor,), as depicted in Fig. 1b. The resistive sensor and the tuning capacitor are considered as ideal components. Fig. 1c is an example of Z real part depending upon R_x in the case of the resonance frequency of the sensing part (f_{r2}) lower than the one of the readout part (f_{r1}). The distance between the two coils affects the amplitude of *Re(Z)*: the greater is the distance, the lower is the sensitivity of the wireless system. To simplify the *Re(Z)* formula, the following assumption were considered:

- R_x is greater than one kiloohm;
- R_2 is negligible because R_2 is usually lower than some tens of ohm;
- the distance between the two coils is kept constant;
- f_{r1} is greater than f_{r2}, to ensure good sensitivity of the measurement system for the R_x estimation.

These assumptions allow calculating R_x by using (1), which is obtained from the simplified expression of *Re(Z)* in (2) at the fixed frequency f_w expressed in (3), which corresponds to the self-resonant frequency of the sensing part:

$$R_x = \frac{L_2(Re(Z(f_w))-R_1)}{\beta - C_0\cdot R_2\cdot(Re(Z(f_w))-R_1)} \quad (1)$$

$$Re(Z(f_w)) = \frac{\beta\cdot R_x}{L_2+R_x\cdot C_0\cdot R_2}+R_1 \quad (2)$$

$$f_w = f_{r2} = \frac{1}{2\pi\sqrt{L_2\cdot C_0}} \quad (3)$$

with

$$C_0 = C_x + C_2 \quad (4)$$

$$\beta = \frac{L_M^2}{L_2\cdot n^2} = (Re(Z(f_w))-R_1)\left(\frac{L_2}{R_x}+C_0\cdot R_2\right) \quad (5)$$

where the inductance L_M models the coupling flux between the two coils and n is the ratio between the equivalent number of windings of L_1 and L_2. β can be calculated through a calibration procedure adopting resistors with a known value. This method allows simplifying and optimizing the design of the impedance measurement circuit for the readout coil since the impedance measurement is performed at only one frequency.

B. Coil Design

According to Section IIA, the estimation of R_x can be obtained by measuring *Re(Z)* of the wireless system at f_w. In order to optimize the design of the equipment for impedance measurements, f_w is preferred to be lower than f_{r1} [9]. For example, the most common impedance/gain-phase analyzers are capable of measuring impedance up to 20/110 MHz. Furthermore, the proposed lumped parameter circuit model could not be valid for greater self-resonance frequencies.

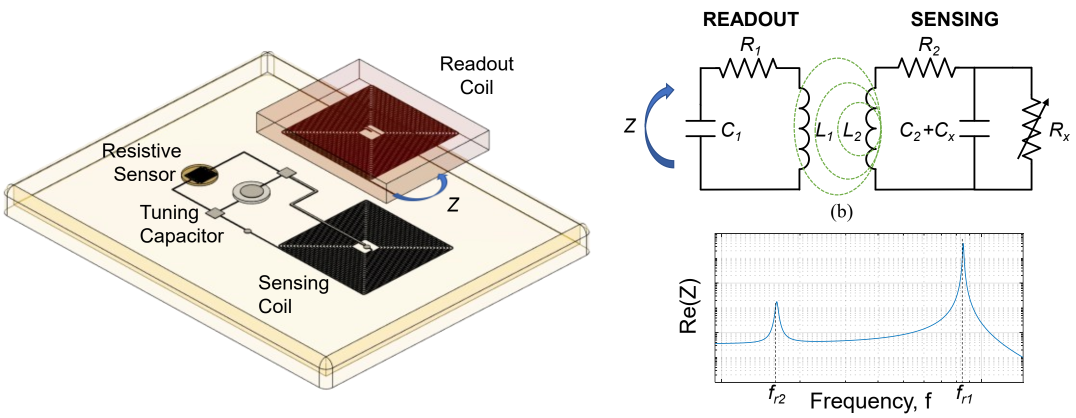

(a) (c)

Fig. 1. (a) Schematic illustration of a smart lid for smart packaging. A resistive sensor is measured through the reading of the impedance of a readout coil, which is coupled with the sensoing coil connected to the resistive sensor. (b) Lumped parameter circuit model of passive telemetric measurement system (c) Typical frequency response of the passive telemetric measurement system when the self-resonance frequency of the sensing coil is lower than of the one of the readout coil.

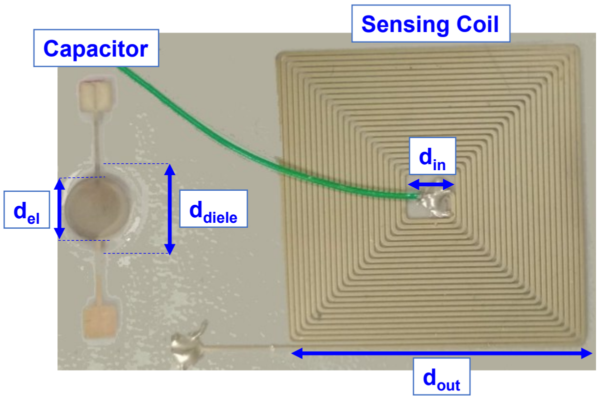

Fig. 2. Printed tuning capacitor and sensing coil.

According to (3), in order to reduce the value of f_w, the coil should be designed with the greatest inductance L_2.

A flat coil in the shape of a spiral is preferred for printed devices because it allows an easier optimizing of its geometry and aspect ratio [13]. Among the most typical geometries (circular, square, hexagonal, and octagonal) for spiral coils, the square spiral coil (an example is shown in Fig. 2) has the highest inductance for the same occupied area, as demonstrated in [14]. For inductance calculation, the modified Wheeler formula could be used for square spiral coil

$$L = 2.34\frac{n^2 d_{avg}}{1+2.75\rho} \tag{6}$$

where n is number of turns, d_{avg}=0.5(d_{out} + d_{in}) and ρ=(d_{out} - d_{in})/ (d_{out} + d_{in}). d_{out} (the outer side of the coil) is usually defined by the constraints final application because it defines the encumbrance of the coil: even if a large area allows increasing L, it could be not compatible with the available printing area of the object. Since the coil will be printed by means of AJP, which is an additive technique, the corners will be smoothed to ensure smooth motion control of the printer and a uniform deposition along the printed path.

The optimization of L implies an increase of the coil resistance according to Ohm's law

$$R = \rho_{coil}\frac{l}{wt} \tag{7}$$

where ρ_{coil} is the resistivity of the conductive material of tracks, w is the width of the tracks, t is the thickness and l is the total length of the spiral track and could be expressed as

$$l \cong 4n(d_{out} - (s+w)(n-1)) \tag{8}$$

where s the spacing of the tracks.

As assumed in Section IIA, R should be kept low (up to some tens of ohms): a good practice is the increase of the thickness t or the use of conductive material with low resistivity.

The design of the coil (Fig. 2) started from the definition of d_{out} equal to 27 mm, because it defined a reasonable printing area for smart packaging applications. d_{in} was fixed to 4.5 mm due to the need to manually attached the wire to the internal pad of the coil. n was set to 23, because in [9] the self-resonant frequency on a coil with these same characteristics resulted lower than 40 MHz. The final dimensions are listed in Table I

Since AJP is capable of depositing layer with a thickness in the range 0.1-2 µm, the printing of the pattern would be repeated several times to increase the thickness t and thus to reduce R. The number of overlapped deposition (n_{dep}) was limited to four to ensure thickness uniformity of the printed track.

TABLE I. GEOMETRICAL CHARACTERISTICS OF THE PRINTED COMPONENTS AND OF THE READOUT COIL

Property	**Sensing**	**Readout**
Coils Characteristics		
d_{out}, outer side (mm)	27.25	27
d_{in}, inner side (mm)	4.5	4
n, number of windings	23	23
w, Winding width (µm)	250	300
s, Winding spacing (µm)	250	200
n_{dep}, Number of depositions	4	
Capacitor characteristics		
d_{el}, Electrode diameter (mm)	6	
d_{diel}, NOA 81 diameter (mm)	8	
n_{dep}, number of dielectric depositions	3	

C. Capacitor Design

According to (3)-(4), adding a capacitor in parallel to the coil is required to tune the self-resonant frequency of the printed coil. The self-resonant frequency of the printed coil could be tuned at a frequency around 12.5 MHz by printing an external capacitor. Therefore, since the capacitance of C_2 was expected to be lower than 5 pF, a tuning capacitor (the final device is shown in Fig. 2) was designed to reduce the self-resonant frequency of the sensing coil. As depicted in Fig. 2, the tuning capacitor is a parallel plate capacitor with round electrodes. The circle shape of the electrode ensures good uniform deposition by means of AJP. The classical formula of a parallel plate capacitor with round electrodes of diameter d_{el} is

$$C = \varepsilon_0\varepsilon_r\frac{\pi d_{el}^2}{4t_{diel}} \tag{9}$$

where ε_0 is the vacuum permittivity, ε_r is the relative permittivity of the dielectric layer and t_{diel} is the thickness of the dielectric layer between the two electrodes. Some overlapped depositions (n_{dep}) of dielectric ink for a uniform dielectric layer were considered.

By combining (3) and (4), the tuning capacitor was designed to have a capacitance C_x equal to 20 pF when f_{r2} is set to 12.45 MHz. Defined the value of t_{diel} and ε_r (Section IVA) and by applying the inverse formula of (9), the resulting d_{el} was fixed to 6 mm (Table I).

III. MATERIALS AND METHODS

A. Materials

Smart Aerosol Conductive Ink (S-CS61308, Genesink, France), based on silver nanoparticles, was selected because it is suitable for applications requiring high conductivity and high resolution at very low curing temperatures (such as in the case of plastic or paper substrates). The ink was developed to design antennas, conductive tracks, and electrodes even on conformable or flexible substrates. The ink has a viscosity in the range 500-700 mPa·s and it requires to be atomized together with ethanol during the printing process to obtain a better printability and adhesion to the substrate. The expected resistivity is 4.5 10^{-8} Ω cm. NOA 81 (Norland Products Inc., Cranbury, New Jersey, USA), a UV-curable polymer, was selected to obtain the dielectric and insulating layer, as NOA 81 has already been resulted suitable for this type of application in [15]. The viscosity of the ink is 300 mPa·s at 25 °C. A polyester (PET) based substrate (Novele IJ-220) was selected as a substrate for the passive smart antenna because it is widely used for everyday objects. Furthermore, it is compatible with the selected ink and is thermally stable at the curing conditions recommended by the proposed fabrication process. For the prototype, 32 AWG wires were attached to the pads of the inductor and the capacitor by means of a conductive glue (CircuitWorks Conductive Epoxy CW2400) for electrical tests.

B. *Manufacturing process*

The AJ-300 Aerosol Jet Printer (Optomec, Albuquerque, NM, USA) was adopted in the pneumatic atomizer mode to deposit both the silver-based ink and the insulator ink. In the proposed method, the temperature of the platen that translates the substrate in the X-Y direction was fixed at 50 °C to dry the ink during the printing, and the printed speed was fixed at 2 mm/s. Printing process parameters tuned to obtain the desired track width are listed in Table II. Process flows are expressed in the unit standard centimeter cube per minute (SCCM).

We drew the layout of the coil and the capacitor by using AutoCAD software, which can provide an output file to control the printer movements during the manufacturing process. The dimensions of each component, already discussed in Section II, are listed in Table I. The two plates of the capacitor have the same layout, but they are symmetrical. The dielectric layer has a larger diameter to prevent shortcuts between the two plates.

As depicted in Fig. 3, while the inductor was printed in one single step, the capacitor and the track that electrically connect the inner pad of the inductor to one pad of the capacitor required three steps: at first, the silver-based bottom electrode was printed and thermally sintered, then the dielectric layer of the capacitor and the insulating track were printed and UV cured, and finally, the upper electrode and the conductive track were printed and thermally sintered.

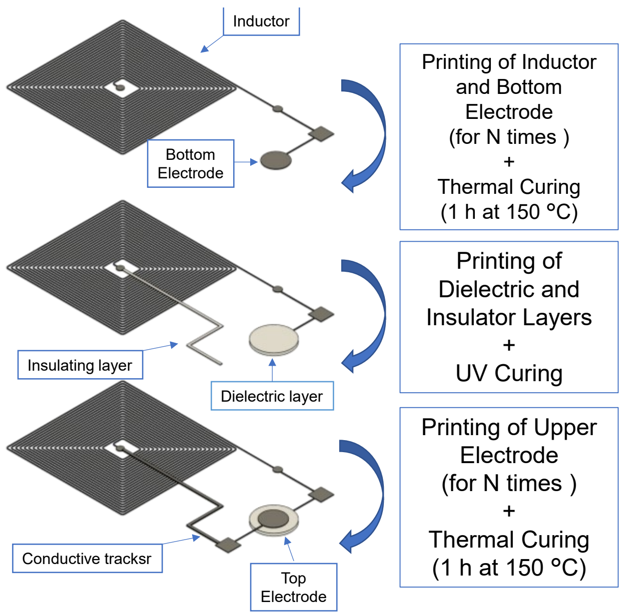

Fig. 3. Manufacturing process for printing coil and capacitor through AJP.

Several consecutive overlapped depositions n_{dep} of silver allowed reducing the resistance of the conductive parts (inductor, tracks, and electrodes) and the capacitance of the resulting capacitor. The deposition of the silver ink was repeated four times for all the conductive parts.

Once the coil, the conductive tracks, and the bottom electrode was printed, the printed prototype was thermally treated at 150 °C for 1 h (as recommended by the manufacturer) in an oven to sinter the ink and to reach the highest conductivity. The next step was the printing of the dielectric/insulating layers by using NOA 81. NOA 81 was cured in-flight during the printing process of the insulator layer by exposing it to a UV light, whose source is optional of the AJ-300 printer.

After the n_{dep} deposition of NOA 81, the upper electrode and the last conductive track were obtained by following the same manufacturing process adopted in the first step.

Finally, the wires were attached to the pads of the inductor and the capacitor.

TABLE II. INKS PROCESS PARAMETERS

Parameter	*S-CS61308*	*NOA81*
Sheath gas flow (SCCM)	400	750
Atomizer gas flow (SCCM)	612	1350
Exhaust gas flow (SCCM)	610	1100

C. *Characterization*

Preliminary tests were performed for determining the geometrical characteristics (profile and width) of the printed layers and the impedance of the final device. The thickness and the width of the printed tracks, as well as the thickness of the dielectric layer of the capacitor, were measured by means of Profilm3D (Filmetrics, San Diego, CA, US). The measurements of the impedance from 100 Hz to 40 MHz were performed by means of an impedance analyzer HP4194A, while the resistance of the resistive device was measured by means of a multimeter HP34401A. The setting and the data acquisition were performed through a Virtual Instrument developed in LabVIEW and a GPIB USB module.

Finally, the printed device was validated with a readout coil fabricated with a Printed Circuit Board (PCB) technique. The telemetric system consists of :

- a square planar coil with copper tracks on a substrate of FR4 glass-reinforced epoxy (geometrical characteristics are listed in Table II).
- the printed coil used as sensing inductor;
- the printed capacitor, connect in parallel to the sensing coil, for tuning the resonance frequency of the sensing device;
- a resistor connected in parallel to the sensing coil and the capacitor. The resistor represents the resistive sensor to be measured.

The two coils were kept in parallel and coaxial position, at a distance of 4 mm.

We considered the measurement of a force resistive sensor (FSR) with a telemetric system as a real application because FSRs can be printed together with the sensing coil and the capacitor on the same substrate by easily modifying the manufacturing process. In order to know the resistance range of the FSR (Tekscan, MA, US) and thus R_x range, different and known weights (100 g, 200g, 500g, and 1 kg) were applied over the sensitive area of FSR and the resistance was measured by mean of a multimeter. The applied force is the product of applied weight and 9.81 N/m^2. For the calibration of the telemetric system, three commercial resistors of known resistance were adopted to find β according to Section IA. The validation of the system was obtained by comparing the resistance obtained through the proposed techniques of Section IA and the one measured by means of the multimeter. For the validation, other commercial resistors of known resistance (ranging from 2.2 kΩ and 560 kΩ) were used.

IV. Results and Discussion

A. Geometrical and Electrical Characterization

The optimization of the printed coil and the tuning capacitor required some preliminary tests to estimate 1) the resistivity, the thickness and the width of the silver tracks and 2) the thickness of the printed dielectric layer.

Nine capacitors (3 samples for each n_{dep}, ranging from one to three) were manufactured according to the manufacturing process described in Section IIIC and their profile was measured. An example of their profile is shown in Fig. 4a. The relative permittivity of NOA-81 resulted in 3.62 by applying the inverse formula of (9) (d_{el} = 6 mm, t_{diel}=$h_{1/2/3}$, $C = C_{1/2/3}$). The error is calculated as the maximum difference between the measured capacitances with the same characteristics and the mean value. The profile of the printed coil (the geometrical characteristics are listed in Table II) was also measured on ten lines 1-mm long (Fig. 4b). The mean thickness (3.15 µm) was

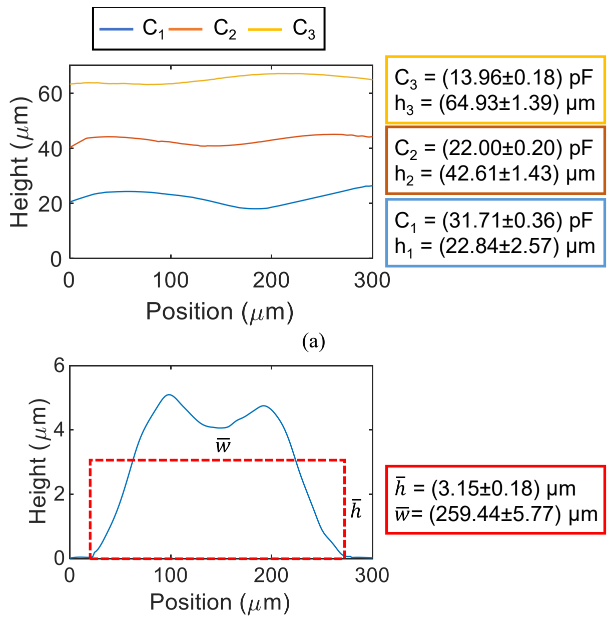

Fig. 4. (a) Profile of NOA81 of three tuning capacitors having different numbers of deposition (from 1 to 3), indicated in the subscript. On the right the mean value of the capacitance and of the height (the error is the deviation standard calculated on ten profile) (b) Profile of the printed lines of the coil. On the rigth the mean value of the height and the mean width.

calculated averaging the ratio between the area of the acquired profiles and the mean width (259.44 µm). The resistivity ρ_{coil} matches the value declared by the manufacturer. It resulted in 4.6 10^{-8} Ωm by considering the resistance R measured on 10 lines 10-mm long and by applying the inverse formula of (7). A printed coil and one capacitor of 14.14 pF (n_{dep} = 3) were connected in parallel and the impedance of the resulting system acquired in the range of 100 – 40 MHz to find the equivalent lumped parameter circuit model. Also the impedance of the readout inductor was acquired.

TABLE III. ELECTRICAL CHARACTERISTICS OF

Property	Sensing	Readout
L, Equivalent inductance (µH)	8.24	7.44
R, Equivalent resistance (Ω)	87	24.16
C, Equivalent capacitance (pF)	19.23	2.79
f_r, Self-resonance frequency (MHz)	12.45	35

B. Calibration of the Telemetric System

The final range of R_x was determined from the results of the FSR characterization. The correlation between the applied force and the measured resistance is shown in Fig. 5, and it was found experimentally according to the procedure described in Section IIID. The resistance of FSR is infinite when no load is applied and it drops to 460 kΩ for applied weight greater than 100 g. For 1 kg the resistance drops to 20 kΩ. For the calibration procedure of the telemetric system, three commercial resistors of values 5606 Ω, 46123 Ω, 269300 Ω were connected to the sensing part of the system for the calculation of β. The acquired real part of the impedance read at the terminals of the readout coil is shown in Fig. 5. The measurements were repeated three times, with good repeatability (the maximum difference between the measurement taken at the same frequency was lower than 5 Ω). By reading $Re(Z)$ at f_w = 12.45 MHz and by applying (5), β resulted 6.36 µH, 6.29 µH, and 6.32 µH when R_x is 5606 Ω, 46123 Ω, 269300 Ω, respectively.

C. Validation of the Telemetric System

For the validation test, other commercial resistors were connected to the sensing part to validate the system. As shown in Fig. 6, the frequency where the real part of the impedance is maximum (f_2) shifted and for this reason β =6.36 µH was used for $Re(Z(f_w))$ lower than 1500 Ω, β =6.29 µH was used for $Re(Z(f_w))$ between 1500-1700 Ω, β =6.32 µH was used for $Re(Z(f_w))$ greater than 1700 Ω. The results are shown in Fig. 7:

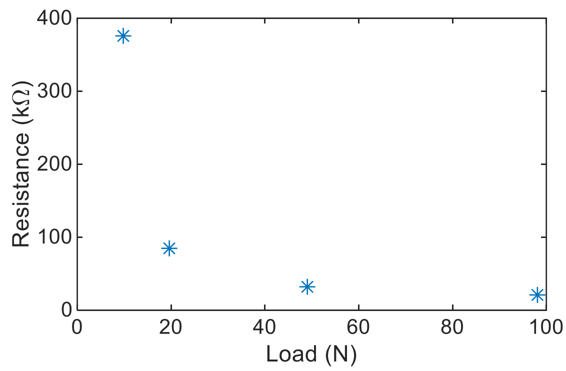

Fig. 5. (a) Characterization of a FSR by changing the applied load (by using known weight from 100 g to 1 kg) over the sensitive area.

the value of the commercial resistors calculated by implementing the proposed technique (y-axis) was correlated with the value measured by means of the multimers before the experiment (x-axis). The maximum deviation of R_x from the reference curve is lower than 6%, despite the large range of the resistances, which causes a shift of f_2 with respect to f_{r2}.

V. CONCLUSIONS

The fabrication of sensors and electronic devices directly onto the surface of the objects represents a new frontier to fabricate smart objects, which can be used in different scenarios (industry, agriculture, healthcare, smart city management, etc.). The passive telemetric method is a valid solution to interrogate the passive sensors without the integration of complex electronic circuits and batteries on the objects. The only components on the object are the sensor, the sensing coil, and an optional capacitor. This is a viable solution for smart packaging, to reduce costs, encumbrance and complexity.

In this work, a manufacturing process to fabricate the coil and the tuning capacitor was proposed. A preliminary study of the components was described in order to fabricate a sensing device with the self-resonant frequency of 12.45 MHz, compatible with the most typical impedance analyzers. The resistivity and the permittivity of the involved ink were

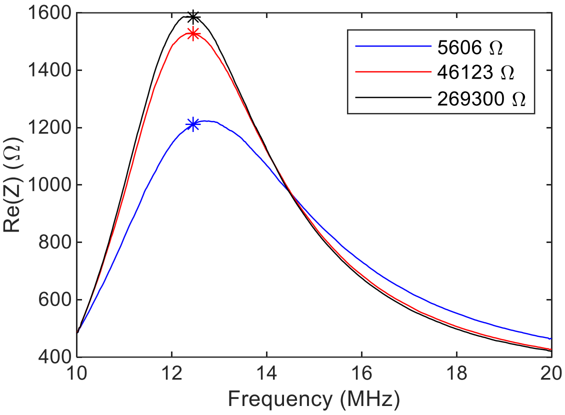

Fig. 6. (a) Real part of the impedance measured at the terminal of the readout coil for known resistor (R_x is indicated in the legend). The star-like symbols correspond to the real part of the impedances at the frequency f_{r2}.

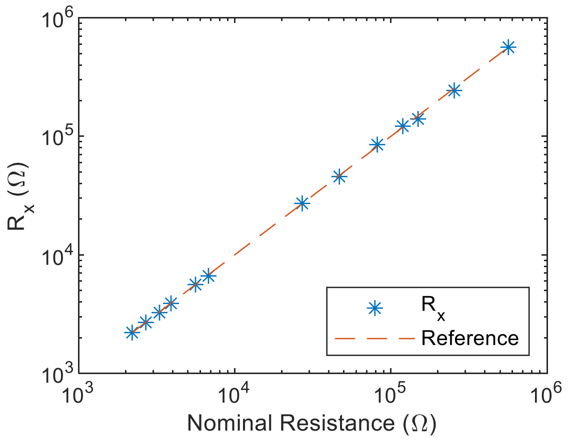

Fig. 7. (a) Validation of the telemetric system by changing the value of R_x from 2.2 kΩ to 560 kΩ (the measured values by means of a multimeter are on x axis). Rx calculated by applying (1) is on y axis.

evaluated as well as the thickness of the deposited materials, in order to support the design of the coil and of the capacitor. Finally, the printed devices were adopted in a telemetric system to validate the proposed solution. The measurement of the resistance deviates from its nominal value of 6% at maximum, when the resistive sensor ranges from 2.2 kΩ and 560 kΩ.

In the future, the fabrication of the electronic components (the resistive sensor, the coil, and the inductor) directly on an object will be proposed and validated. A further study that considers the distance between the two coils or the type of surface will be proposed to optimize the design of the entire passive telemetric system.

REFERENCES

[1] J. Jansen and A. van der Merwe, "A Framework for Industrial Internet of Things," in *Responsible Design, Implementation and Use of Information and Communication Technology*, 2020, pp. 138–150.

[2] S. Selvaraj and S. Sundaravaradhan, "Challenges and opportunities in IoT healthcare systems: a systematic review," *SN Appl. Sci.*, vol. 2, no. 1, pp. 1–8, 2020, doi: 10.1007/s42452-019-1925-y.

[3] T. A. Khoa *et al.*, "Designing Efficient Smart Home Management with IoT Smart Lighting: A Case Study," *Wirel. Commun. Mob. Comput.*, vol. 2020, 2020, doi: 10.1155/2020/8896637.

[4] M. Silverio-Fernández, S. Renukappa, and S. Suresh, "What is a smart device? - a conceptualisation within the paradigm of the internet of things," *Vis. Eng.*, vol. 6, no. 1, 2018, doi: 10.1186/s40327-018-0063-8.

[5] M. Borghetti, E. Cantù, E. Sardini, and M. Serpelloni, "Future Sensors for Smart Objects by Printing Technologies in Industry 4.0 Scenario," *Energies*, vol. 13, no. 22, 2020, doi: 10.3390/en13225916.

[6] G. Huang *et al.*, "A simple ultrasensitive electrochemical biosensor for simultaneous determination of dopamine, uric acid and ascorbic acid based on β-cyclodextrin/selenium doped carbon quantum dots modified glassy carbon electrode," *Int. J. Electrochem. Sci.*, vol. 15, pp. 9888–9901, 2020, doi: 10.20964/2020.10.47.

[7] O. Urbano *et al.*, "Cost-effective implementation of a temperature traceability system based on smart RFID tags and iot services," *Sensors (Switzerland)*, vol. 20, no. 4, 2020, doi: 10.3390/s20041163.

[8] G. Fuertes, I. Soto, R. Carrasco, M. Vargas, J. Sabattin, and C. Lagos, "Intelligent Packaging Systems: Sensors and Nanosensors to Monitor Food Quality and Safety," *J. Sensors*, vol. 2016, 2016, doi: 10.1155/2016/4046061.

[9] M. Bona, M. Borghetti, E. Sardini, and M. Serpelloni, "Telemetric Technique for Passive Resistive Sensors Based on Impedance Real Part Measurement at Fixed Frequency," *IEEE Trans. Instrum. Meas.*, vol. 67, no. 9, pp. 2160–2168, 2018, doi: 10.1109/TIM.2018.2811279.

[10] M. Z. Xie, L. F. Wang, L. Dong, W. J. Deng, and Q. A. Huang, "Low Cost Paper-Based LC Wireless Humidity Sensors and Distance-Insensitive Readout System," *IEEE Sens. J.*, vol. 19, no. 12, pp. 4717–4725, 2019, doi: 10.1109/JSEN.2019.2901004.

[11] Y. Ji, Q. Tan, H. Wang, W. Lv, H. Dong, and J. Xiong, "A Novel Surface LC Wireless Passive Temperature Sensor Applied in Ultra-High Temperature Measurement," *IEEE Sens. J.*, vol. 19, no. 1, pp. 102–112, 2019, doi: 10.1109/JSEN.2018.2872915.

[12] M. Xie, L. Wang, L. Dong, W. Deng, and Q. Huang, "Low Cost Paper-Based LC Wireless Humidity Sensors and Distance-Insensitive Readout System," *IEEE Sens. J.*, vol. 19, no. 12, pp. 4717–4725, 2019, doi: 10.1109/JSEN.2019.2901004.

[13] U. M. Jow and M. Ghovanloo, "Design and optimization of printed spiral coils for efficient transcutaneous inductive power transmission," *IEEE Trans. Biomed. Circuits Syst.*, vol. 1, no. 3, pp. 193–202, 2007, doi: 10.1109/TBCAS.2007.913130.

[14] S. S. Mohan, M. D. M. Hershenson, S. P. Boyd, and T. H. Lee, "Simple accurate expressions for planar spiral inductances," *IEEE J. Solid-State Circuits*, vol. 34, no. 10, pp. 1419–1420, 1999, doi: 10.1109/4.792620.

[15] M. Serpelloni, E. Cantù, M. Borghetti, and E. Sardini, "Printed Smart Devices on Cellulose-Based Materials by means of Aerosol-Jet Printing and Photonic Curing," *Sensors*, vol. 20, no. 3, p. 841, Feb. 2020, doi: 10.3390/s20030841.